2009 International Nuclear Atlantic Conference - INAC 2009
Rio de Janeiro,RJ, Brazil, September27 to October 2, 2009
ASSOCIAÇÃO BRASILEIRA DE ENERGIA NUCLEAR - ABEN
ISBN: **978-85-99141-03-8**

COMPUTED RADIOGRAPHY SIMULATION USING THE MONTE CARLO CODE MCNPX

S.C.A. Correa[1,2], E.M. Souza[1,3], A.X. Silva[1], D.H. Cassiano[4], R.T. Lopes[1]

[1] Programa de Engenharia Nuclear – COPPE
Universidade Federal do Rio de Janeiro
Ilha do Fundão, Caixa Postal 68509
21945-970 Rio de Janeiro, RJ
scorrea@con.ufrj.br

[2] Centro Universitário Estadual da Zona Oeste, UEZO
Av. Manoel Caldeira de Alvarenga, 1203
23070-200 Rio de Janeiro, RJ

[3] Departamento de Geologia, Instituto de Geologia
Universidade Federal do Rio de Janeiro
Ilha do Fundão, 68509
21945-970 Rio de Janeiro, RJ

[4] Instituto de Radioproteção e Dosimetria/CNEN
Av. Salvador Allende, s/n - Recreio – 22780-160
Rio de Janeiro, RJ - Brasil

ABSTRACT

Simulating x-ray images has been of great interest in recent years as it makes possible an analysis of how x-ray images are affected owing to relevant operating parameters. In this paper, a procedure for simulating computed radiographic images using the Monte Carlo code MCNPX is proposed. The sensitivity curve of the BaFBr image plate detector as well as the characteristic noise of a 16-bit computed radiography system were considered during the methodology's development. The results obtained confirm that the proposed procedure for simulating computed radiographic images is satisfactory, as it allows obtaining results comparable with experimental data.

1. INTRODUCTION

In recent years a growing interest has been witnessed in simulating x-ray images in a number of applications [1-5]. The key reason for this interest resides in the ability to study how changes in relevant operating parameters may affect the x-ray image's quality without the restrictions imposed by the experimental procedure and without causing exposure to radiation.

One of the methods widely employed for simulating images has been the Monte Carlo method owing to the stochastic nature of radiation emissions, transportation, and detection processes. Among the main general-purpose codes based on the Monte Carlo method, the MCNPX (Monte Carlo N-Particle eXtended) code has been one of the sole ones to provide specific functions to simulate x-ray images [6]. However, though the MCNPX code provides specific commands to simulate x-ray images, a number of procedures still have to be performed to make the latter compatible with images obtained by experimental detectors. Previously we have developed a methodology for digital radiography simulation using the Monte Carlo code MCNPX [7]. This methodology takes into account the energy response by a BaFBr sensitive material image plate detector and the linear response curve of a 16 bit

digital system. However the presence of system noise such as electronic noise was not considered.
With this in mind, the purpose of this paper is to propose a procedure for simulating computed radiographic images using the Monte Carlo code MCNPX takes into account the sensitivity curve of the BaFBr image plate detector, as well as the characteristic noise of a 16-bit computed radiographic system.

2. MODELING SYSTEM

2.1 Modeling the Image Plate Detector

The MCNPX code [6] employs a set of point detectors close enough to one another to create an image based on the fluence of particles passing through each detector. Once the image function is activated, MCNPX creates a virtual two-dimensional pixel matrix perpendicular to the particle beam's central axis, at a selected distance from the test subject, where millions of point detectors may be created, one detector for each pixel. These pixels work like cells in which the particles will be counted or their energies recorded. An individual pixel in this matrix represents one pixel in the simulated image.
Though the MCNPX's radiographic function represents a significant advance in the outlook for image studies with this code, there are still limitations. One of the main ones is because the pixel matrix cannot be inserted in a spreading material [6]. This image function feature limits MCNPX to studies with ideal detectors, in which atomic and/or nuclear radiation reactions with the substances composing the detector are not considered.
The solution employed in this paper to simulate the energy response by a BaFBr sensitive material image plate detector, was the use of the MCNPX code's DE/DF command. This command is used to correlate data obtained in the simulation with other quantities of interest, such as for example fluence conversion factors for doses through the introduction of a multiplier dependent on energy. The term DF is equal to a response function of a specific material for the incident radiation's DE energies, in MeV, in which each simulation result (fluence) is multiplied by a value of the DF conversion factor equal to the incident radiation's DE energy. Energy values outside of the range defined in the DE/DF command are interpolated between any of the higher or lower energy values contained in the respective sequences.
The sensitive material's DF response function was obtained by means of individual simulations on non-diverging mono-energetic beams originating from a plane source, depositing energy per mass unit (MeV/g) on a BaFBr block of 5.1 $g.cm^{-3}$ in density [8], 0.03 cm thick, and an area equal to the source. The energy interval used was of 0.002 to 1 MeV. Figure 1 shoes the DF distribution based on the DE obtained in the simulation.
The discontinuity region in the curve is equal to the BaFBr material's k fluorescence peak. The value obtained in the simulation was 37 keV, showing a 1.07% relative error as compared to the value provided in literature, 37.4 keV [8].
Once the DE and DF values were obtained, they were grouped and inserted into the entry files for modeling x-ray trials with the MCNPX code. Hence, the results obtained in the detecting grid, in fluence (cm^{-2}), are now correlated to the DE values and multiplied by the respective DF values ($MeVxcm^2/g$), thus being modified to energy absorbed per unit of mass (MeV/g) in the BaFBr material.

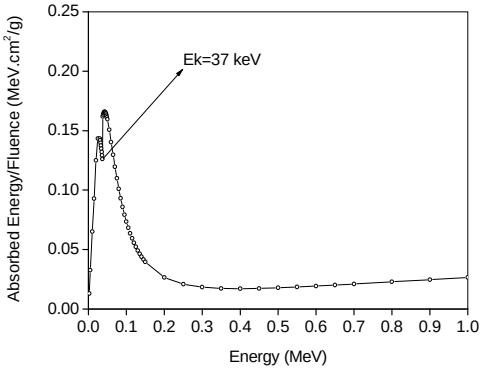

Figure 1. Sensitive BaFBr material's response function. The values obtained were normalized by means of the fluence of photons emitted by the source.

2.2 Consideration of the Density of the Photons Incident on the Detector

In the MCNPX code, the images obtained with the x-ray function as well as all the other quantities calculated by the code are normalized to one particle emitted by the source [6,9]. As the signal produced in an image plate detector depends on the total energy absorbed by the sensitive material, and as a result the latter will vary with the number of photons incident on the detector, a procedure to consider the density of photons incident on the simulated detector had to be developed.

During a first stage, the procedure developed consisted in normalizing the energy values absorbed in the simulated image plate detector by air kerma incident on it (obtained with the MCNPX code). Later, in a subsequent stage, the normalized values of the energy absorbed in the simulated detector were multiplied by air kerma incident on a real image plate detector, as shown in Equation 1, in which air kerma incident on the real detector has to be obtained in the same exposure conditions used in the simulation.

$$H_{S,T} = \frac{DD}{KS} KE \tag{1}$$

in which $H_{S,T}$ is a energy absorbed in the sensitive BaFBr material simulated detector considering the number of photons incident on the detector, *DD* is the energy absorbed in the BaFBr detector for one particle, *KS* is air kerma incident on the BaFBr detector for one particle, and *KE* is air kerma incident on the BaFBr detector for *N* particles.

2.3 Calibrating the Simulated Detector's Pixels

In order to correlate the simulated detector's pixel values with those of a real 16-bit detector, experimental images of a homogeneous aluminum plate measuring 10 x 10 cm², 0.5 cm thick, and 99% degree of pureness, were obtained for several values of air kerma incident on the detector. The air kerma values were varied by changing the product of current and exposure time (mAs), with an 80 kV voltage. In order to measure air kerma, an ionizing chamber was positioned in the region where the image detector was located. The air kerma values considered consisted in the arithmetical average of three measurements. Table 1 shows the main information from the equipment employed.

Table 1. Description of the equipments employed to obtain experimental images of the aluminum plate in order to calibrate the simulated detector's pixel values.

Equipments	Specifications
X-ray equipment	Fein Focus FXS-100.10 Maximum tube voltage: 100 kV Maximum current: 1 mA Target angle: 22^0 Focal spot size: 10 μm Filtration: 0,0
Radiation measurement system	Radcal Model: 9015 Ionization chamber: 10x5-6
Image plate detector	BaFBr Scanner: GE CR TOWER Resolution: 16 bits.

Images of an aluminum plate (2.699 g/cm³ in density) measuring 10 x 10 cm² and 0.5 cm thick were also simulated. The x-ray source considered consisted in a 10 μm diameter disk, collimated into a cone of directions by using the variance reduction technique called source biasing [6,9]. The distributions in x-ray energy used as entry parameters to simulate radiation beams were obtained with a SRS-78 software [10] using a tungsten anode with a 22º angularity and 80 kV voltage applied to the tube. No radiation beam filtration was considered. The modeled source sought to reproduce the key features of the x-ray equipment described in Table 1.

In order to obtain simulated images, a detector with 100 μm in resolution was considered. Air kerma incident on the detector was obtained by means of a point detector (F5 command) [6,9] positioned in line with the radiation beam's central axis and 5 cm from the aluminum plate. DE/DF conversion factors provided by ICRP51 [11] were employed to convert fluence into air kerma.

The simulated images pixel values were normalized through simulated air kerma and multiplied by air kerma obtained experimentally. This procedure was performed for each experimental air kerma value obtained by changing the product of current and exposure time. Later, the average arithmetical pixel values in the simulated detector were plotted based on the average arithmetical pixel values in the experimental detector, as shown in Figure 2.

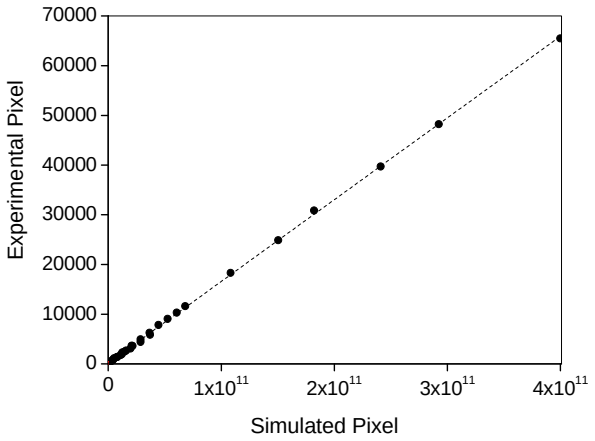

Figure 2. The average arithmetical pixel values in the simulated detector based on the average arithmetical pixel values in the real detector. Data obtained for different values of air kerma incident on the detector.

Each average arithmetical pixel value in the experimental detector was obtained considering five regions in the image. The maximum change among the average values in the five regions studied was below 3% of the total average.
Adjusting a curve between the average arithmetical pixel values in the simulated detector and the average arithmetical pixel values in the experimental detector, it was possible to obtain an equation to make the pixel values in the simulated detector (*PS*) compatible with the real 16-bit image plate detectors (*VP*).

2.4 Description of the Image Plate System's Noise

The maximum signal to noise ratio (SNR) [12] in any image system occurs when the x-rays are absorbed by the detector's sensitive material. If the image system's signal to noise ratio is essentially determined in this stage, it is said that the image system's performance is limited by quantum noise [8].
As quantum noise is produced by independent and random interactions of the x-ray photons with the detector, it may be described quantitatively by means of Poisson's statistical distribution [12]. In the case of a beam emerging from a homogeneous body of constant thickness, changes in the energy absorbed owing to the radiation's random interaction nature with the detectors sensitive material (quantum noise) may be estimated by [12]:

$$R_q = \sqrt{\mu} \tag{2}$$

in which μ is the average energy absorbed of the homogeneously exposed pixels, and R_q is quantum noise.
The signal to noise ratio of a system limited solely by quantum noise may be described as:

$$SNR = \frac{\mu}{\sqrt{\mu}} \tag{3}$$

However, in a real image system, inevitably the signal to noise ratio will be reduced by the signal's processing in the several electronic devices that compose the detector. This reduction occurs in particular owing to electronic noise [8].
Differently from system with linear amplification, in which electronic noise does not depend of energy absorbed in the detector [13], image plate detectors tend to increase electronic noise with the energy absorbed. This behavior occurs in particular due to the use of photo-multipliers in the signal amplification process. The greater the energy absorbed in the sensitive material, the greater will be the number of electrons originating from the photo-cathode (primary electrons). As a result, the electronic noise from the capacitance of the dinode will be greater, as well as the fluctuation in the dark current, thus causing an increase in electronic noise with the energy absorbed in the detector [8, 14].
Hence, considering that an image plate detector's electronic noise is proportional to the energy absorbed, the following relation may be made:

$$R_e = \gamma\sqrt{\mu} \tag{4}$$

in which μ is the average energy absorbed in the homogeneously exposed pixels, R_e is electronic noise, and γ is a multiplicative factor that changes with the energy absorbed in the detector.

The digital x-ray image's total noise is the result of the sum of quantum noise and electronic noise, as shown in Equation 5 [13]. Using Equations 2 and 4, total noise may also be estimated through of the Equation 8.

$$R = R_q + R_e \tag{5}$$

$$R = \sqrt{\mu} + \gamma\sqrt{\mu} \tag{6}$$

$$R = (1+\gamma)\sqrt{\mu} \tag{7}$$

$$R = \alpha\sqrt{\mu} \tag{8}$$

in which R is the system's total noise, and $\alpha = (1 + \gamma)$ is a multiplicative factor that changes with the energy absorbed in the detector.

The use of an multiplicative factor (α) as shown in Equation 8 makes it possible to estimate the image's total noise based on quantum noise.

The total noise may also be estimated by means of the digital image's pixel value standard deviation. The standard deviation quantifies the pixel values' changes or dispersion around an average value [15].

In order to discover the multiplicative factor that changes with the energy absorbed on the detector, the same experimental arrays found in Figures 3 (a) and (b) were devised. Through this array several experimental images of the homogeneous aluminum plate measuring 10 x 10 cm², 0.5 cm thick, and 99% degree of pureness, were obtained for several values of air kerma incident on the detector. The air kerma values were varied changing the product of current and exposure time, and the voltage applied to the x-ray tube, which varied from 50 kV to 90 kV. By means of images obtained experimentally, the pixel value arithmetical average and standard deviation were obtained.

By using the experimental image's pixel value arithmetical average and standard deviation, it was possible to estimate quantum noise and total noise. Quantum noise was calculated by means of the square root of the image's average pixel values ($\sqrt{\mu}$), and total noise through the image's pixel value standard deviation. Bearing this in mind, quantum noise and total noise for the several experimental images were calculated based on air kerma incident on the image detector. Figure 3 shows the behavior of both noises.

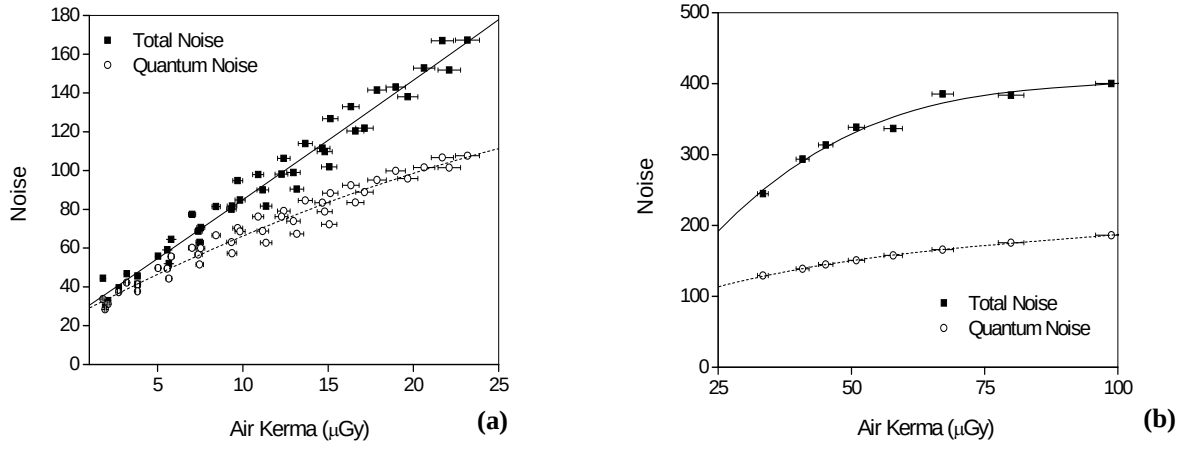

Figure 3. Quantum noise and total noise based on air kerma incident on the BaFBr image detector. In (a), noises for the air kerma range from 1 to 25 μGy, and (b) noises for the air kerma range from 25 to 100 μGy. Data obtained by means of experimental images of an object with a homogeneous composition and constant thickness.

Figure 3 shows that quantum noise and total noise increase with air kerma incident on the image detector, and the increase is shown for the more intense total noise. By means of the ratio between the total noise and quantum noise curves, it was possible to arrive at the α multiplicative factor based on air kerma incident on the detector. Figure 4 shows the α multiplicative factor based on air kerma in the detector.
By adjusting a curve to the values shown in Figure 4, it was possible to obtain an equation that describes the multiplicative factors based on air kerma (K). By means of this equation, it is possible to estimate total noise (R) based on quantum noise (R_q).

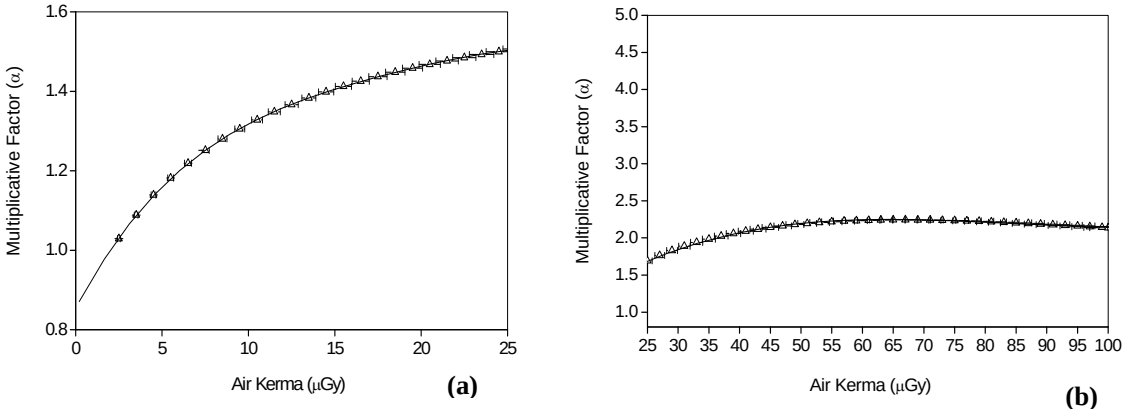

Figure 4. The α multiplicative factor based on air kerma in the detector. In (a), the multiplicative factor for the air kerma range from 1 to 25 µGy, and (b) the multiplicative factor for the air kerma range from 25 to 100 µGy.

2.5 Inserting an Image Plate System's Noise in the Simulated Image

Each pixel's noise amplitude in the simulated image was obtained by discretizing Equation 8 for each pixel individually, as shown in Equation 9.

$$R_i = \alpha\sqrt{s_i} \tag{9}$$

in which R_i is the total noise amplitude in the simulated image's i pixel, s_i is the i pixel's value, α is the multiplicative factor for each specific value of air kerma incident on the image detector.
The final simulated image with noise is obtained with the use of the Box-Muller method. This method creates random variables in accordance with a normal distribution [16, 17]. Equation 10 shows how the Box-Muller distribution is created.

$$z = \sqrt{-2\log u_1}\cdot\cos(2\pi\cdot u_2) \tag{10}$$

The u_1 and u_2 variables are random numbers uniformly distributed in [0.1], and z is a random variable that complies with a normal distribution. The z random variable obtained is then multiplied by the total noise's amplitude (R_i) and added to each pixel value (VP) in the simulated image according to the equation below:

$$VP = s_i + zR_i \tag{11}$$

in which VP is the final value of the pixel changed by noise R_i.

2.6 Post-Processing of Simulated Images

As seen previously, after creating the data by means of the MCNPX code, a number of stages are required to obtain a computed simulated x-ray image. To simplify this process, a post-processing program was devised with the LABVIEW (*Laboratory Visual Instrument Engineering Workbench)* software, version 8.2, in which the all stages shown were considered. The post-processing program's interface is shown in Figure 5.

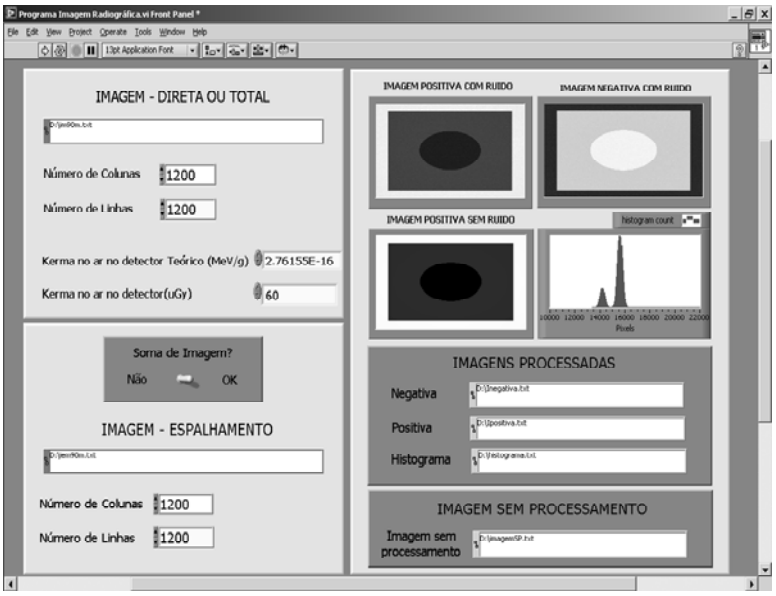

Figure 5. Interface of the simulated image post-processing program.

3. RESULTS

In order to validate the modeled detection system, two analyses were performed: one for the pixel values and one of the images obtained from a test object.

3.1 Analyzing the Pixel Values obtained with the Modeled Detection System

In order to perform this analysis, images were obtained of aluminum plates from 0.05 to 0.55 cm in thickness, and images of polystyrene plates of 1 to 5 cm in thickness. The plates employed measured 10 x 10 cm², and the distances adopted between the x-ray source and the detector, and between the aluminum plate and the detector were of 1 m and 5 cm respectively. The irradiation technique employed was of 80 kV, 63 μA and 10 s, and the respective values of air kerma incident on the detector were measured for each exposure.
The simulated images were acquired considering the same irradiation geometry employed in obtaining the experimental images. The simulated detector's resolution were of 100 μm.
The equipment employed in the experimental stage are equal to those specified in Table 1, and the modeled x-ray source used was the same employed in the previous stages.
Figures 6 and 7 show a comparison between the pixel values obtained by means of the experimental images and the simulated images for the polystyrene and aluminum plates respectively. The simulated pixel values were obtained through the simulated image's arithmetical pixel average, and the experimental pixel values were obtained through the arithmetical pixel average in five different regions in the experimental image. The maximum

change among the average values in the five regions under consideration in the experimental image was less than 8% of the total average for the aluminum and polystyrene plates.
A 7.94% maximum percent error for the polystyrene and aluminum plates may be seen in Figures 6 and 7 between the pixel values of the experimental and simulated images, which evidences the good concordance between the experimental and simulated image acquisition systems in obtaining images of materials of different compositions and thicknesses.
In order to confirm whether there is a good concordance between the pixel values obtained experimentally and by means of simulation with a variation of the x-ray technique (voltage and current), experimental and simulated images were also obtained of an aluminum plate 0.5 cm thick with different voltage values. The methodology for estimating the simulated and experimental pixel values, and the irradiation geometric configuration were the same as previously employed. Figure 8 shoes the results obtained.
The results shown in Figure 8 confirm that even with varied x-ray techniques (voltage) the percent error between the pixel values obtained experimentally and by means of simulation is less than 10%. These results evidence that the detection system simulated in this paper is able to reproduce pixel values close to those obtained with a digital detection system of the 16-bit image plate type.

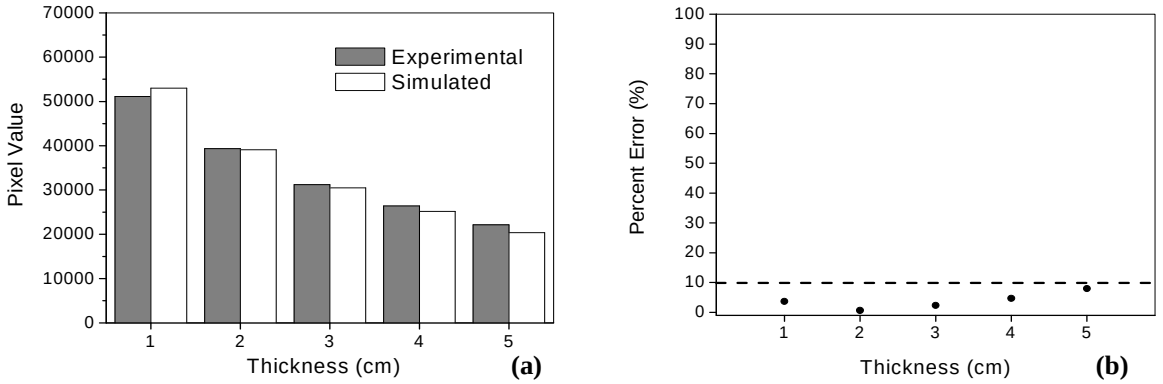

Figure 6. A comparison between the pixel values obtained by means of the experimental images and the simulated images for the polystyrene plates. In (a) pixel values and in (b) percent error.

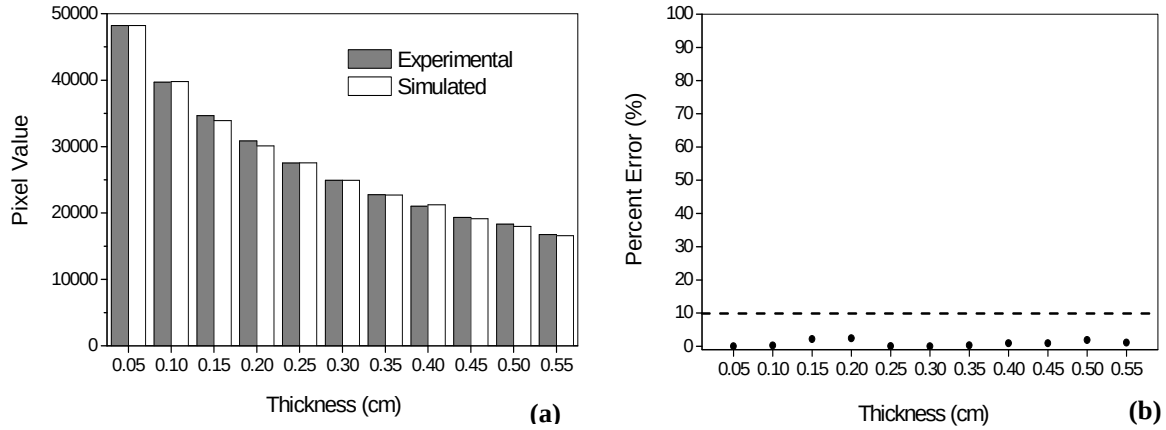

Figure 7. A comparison between the pixel values obtained by means of the experimental images and the simulated images for the aluminum plates. In (a) pixel values and in (b) percent error.

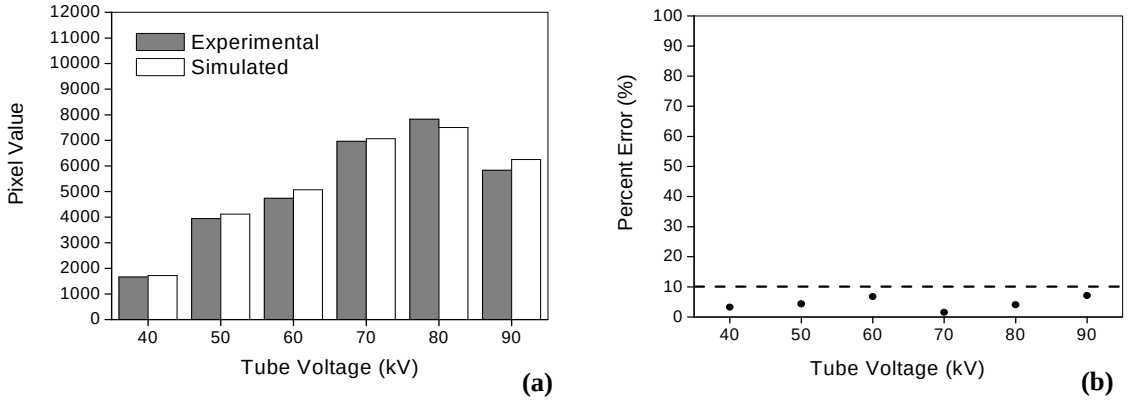

Figure 8. A comparison between the pixel values obtained by means of the experimental images and the simulated images, varying the x-ray techniques employed. In (a) pixel values and in (b) percent error.

3.2 Analyzing Images obtained from a Test Object

In order to perform a more thorough analysis of the simulated image detection system, images of a test object according to the diagram in Figure 9 were simulated and compared with images obtained experimentally. In order to obtain the experimental and simulated images, a 1-meter distance between x-ray source and detector. The distance between detector and object was 0 cm (zero). The simulated detector's resolution was of 100 μm.

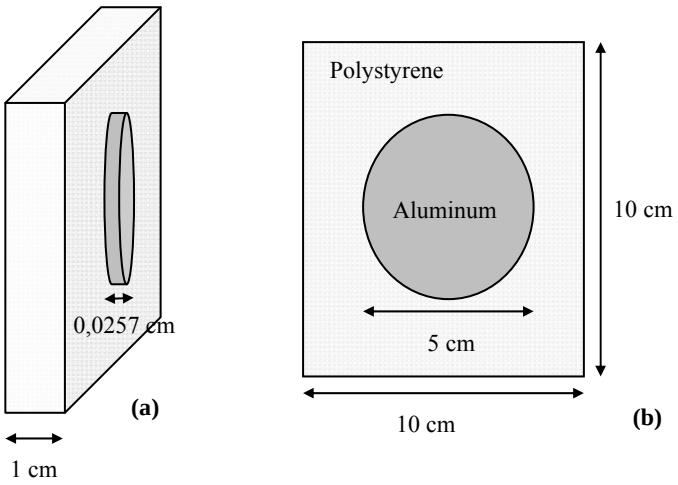

Figure 9. Test object. In (a), a side view and in (b), a front view.

Figures 10, 11, and 12 show images of the test object and its respective profiles, obtain experimentally and by means of simulation using 70, 80, and 90 kV voltages. The images were obtained with air kerma incident on the detector equal to 60 μGy. An Image J software [18] was employed to analyze the images.
A visual comparison of the simulated and experimental images, and their respective profiles shoes that there are similarities between the results.

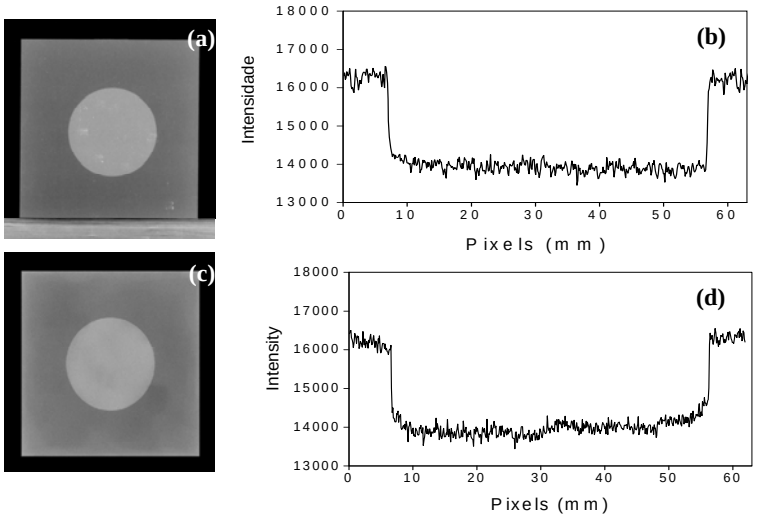

Figure 10. 70 kV images of the test object. In (a), experimental image; (b) experimental image profile; (c) simulated image; (d) simulated image profile.

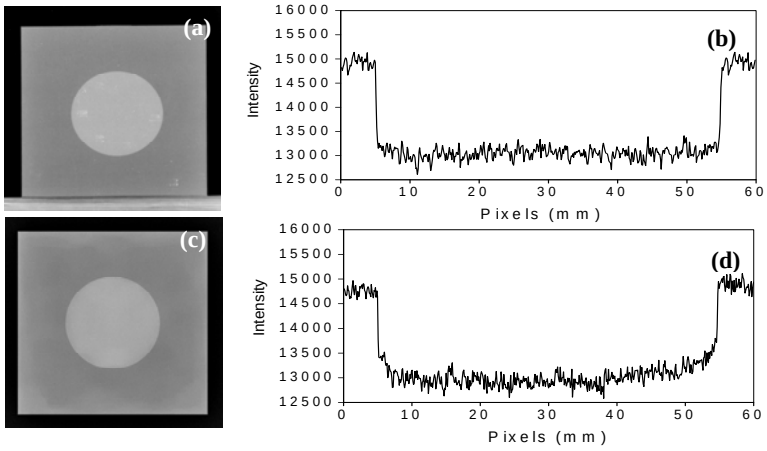

Figure 11. 80 kV images of the test object. In (a), experimental image; (b) experimental image profile; (c) simulated image; (d) simulated image profile.

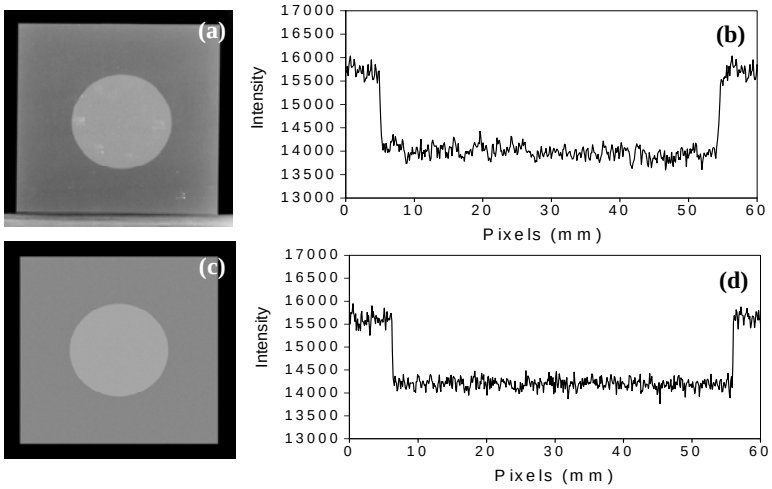

Figure 12. 90 kV images of the test object. In (a), experimental image; (b) experimental image profile; (c) simulated image; (d) simulated image profile.

4. CONCLUSION

The results obtained confirm that the proposed procedure for simulating computed radiographic images using the MCNPX Monte Carlo code is satisfactory, as it allows obtaining results comparable with experimental data.

ACKNOWLEDGMENTS

The authors wish to thank the financial support of the Conselho Nacional de Desenvolvimento Científico e Tecnológico (CNPq) and Fundação Carlos Chagas Filho de Amparo à Pesquisa do Estado do Rio de Janeiro (FAPERJ), Brazil.

REFERENCES

[1] J. Gray, "Three dimensional modeling of projection radiography, in Proceedings of the Review of Progress in QNDE", 7th ed., Plenum Press, New York (1988).
[2] J. Xu, R.M. "Wallingfor,T. Jensen, J. Gray, Recent developments in the X-ray radiography simulation code, XRSIM", in Proceedings of the Review of Progress in QNDE, 13th ed. Plenum Press, New York (1994).
[3] V. Fanti, R. Marzeddu, G. Massazza, P. Randaccio, A. Brunetti, B. Golosio, "A Simulator for X-ray Images", *Radiation Protetion Dosimetry*, pp.350-354 (2005).
[4] M. Sandborg, G. McVey, D.R. Dance, G.A. Carlsson, "Schemes for the Optimization of Chest Radiography Using a Computer Model of the Patient and X-ray Imaging System", *Medical Physics*, pp. 2007-2019 (2001).
[5] M. Sandborg, A. Tingberg, D.R. Dance, B. Lanhede, A. Almen, G. McVey, S. Sund, J. Kheddache, Besjakov, S. Mattsson, L.G. Mansson, G. Alm Carlsson, "Demonstration of correlations between Clinical and Physical Image Quality Measures in Chest and Lumbar Spine Screen-film Radiography", *Br. J. Radiol*., pp. 520-528 (2001).
[6] D.B. Pelowitz, Ed. "MCNPX™ User's Manual". Version 2.5.0., Los Alamos National Laboratory report LA-CP-05-0369, (2005).
[7] E.M. Souza, S.C.A. Correa, A.X. Silva, D.F. Oliveira, R.T. Lopes, "Methodology for Digital Radiography Simulation using the Monte Carlo Code MCNPX for Industrial Applications", *Applied Radiation and Isotopes*, **66**, pp. 587-592 (2008).
[8] J.A. Rowlands, "The Physics of Computed Radiography", *Phys. Med. Biol*., pp. R123-R166 (2002).
[9] J.F. Briesmeister, "MCNP: A General Monte Carlo code for neutron and photon transport", Version 4C, Los Alamos National Laboratory report LA-13709-M, (2000).
[10] K. Cranley, B.J. Gilmore, G.W.A. Fogarty, L. Desponds, "Catalogue of Diagnostic X-Ray Spectra and Other Data", Institute of Physics and Engineering in Medicine Report 48, (1997).
[11] International Commission on Radiological Protection, Data for Use in Protection Against External Radiation, ICRP Publication 51, Oxford: Pergamon Press, (1987).
[12] A.B. Wolbarst, "Physics of Radiology", *Medical Physics Publishing*, 2th ed., Madson, Wisconsin, (2005).
[13] H.P. Chan, K.L. Lam, Y. Wu, "Studies of Performance of Antiscatter Grids in Digital Radiography: Effect on Signal-to-Noise Ratio", *Med. Phys.,* pp. 655-664 (1990).
[14] G.F. Knoll, "Radiation Detection and Measurement", *John Wiley and Sons*, Inc.,3th ed., USA, (2000).
[15] M. Pagano, K. Gauvreau, "Princípios de Bioestatística", 2^0 ed., Pioneira Thomson Learning, Brasil, (2004).
[16] G.E.P. Box, M.E. Muller, "A note on the generation of random normal deviates", *Annals Math. Stat*, pp. 610-611 (1958).
[17] P.A. Moretin, W. Bussad, Estatística Básica, Atual, Brasil, (1986).
[18] W. Rasband, Image J 1.33u. National Institutes of Health, USA, (2005).